JOC The Journal of Organic Chemistry

Article

pubs.acs.org/joc

The Effect of HSAB on Stereoselectivity: Copper- and Gold-Catalyzed 1,3-Phosphatyloxy and 1,3-Halogen Migration Relay to 1,3-Dienes

Jingxing Jiang, Cheng Hou, Shidong Zhang, Zihong Luan, Cunyuan Zhao, and Zhuofeng Ke*

MOE Key Laboratory of Bioinorganic and Synthetic Chemistry, School of Chemistry and Chemical Engineering, Sun Yat-sen University, Guangzhou 510275, P. R. China

Supporting Information

ABSTRACT: The origin of stereodivergence between copper- and gold-catalyzed cascade 1,3-phosphatyloxy and 1,3-halogen migration from α-halo-propargylic phosphates to 1,3-dienes is rationalized with density functional theory (DFT) studies. Our studies reveal the significant role of the relative hardness/softness of the metal centers in determining the reaction mechanism and the stereoselectivity. The relative harder Cu(I/III) center prefers an associative pathway with the aid of a phosphate group, leading to the (*Z*)-1,3-dienes. In contrast, the relative softer Au(I/III) center tends to undergo a dissociative pathway without coordination to a phosphate group, resulting in the (*E*)-1,3-dienes, where the *E* type of transition state is favored due to the steric effect. Our findings indicate the intriguing role of hard−soft/acid−base (HSAB) theory in tuning the stereoselectivity of metal-catalyzed transformations with functionalized substrates.

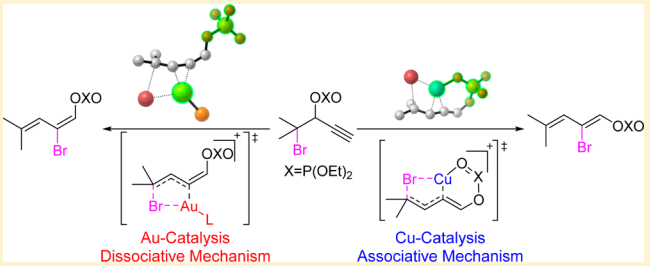

1. INTRODUCTION

The concept of hard and soft acids and bases (HSAB)[1−7] has become a useful tool to analyze and predict the stability and reactivity of metal complexes. The HSAB theory has been widely used in various areas of chemistry,[8−15] like tuning the interaction,[16−19] the reactivity,[12,13,20−23] and the regioselectivity.[13,20,24,25] However, the application of the HSAB concept to control the reaction stereoselectivity is still underdeveloped. Herein, we present a computational study to illustrate a rare example that the HSAB theory plays a crucial role in controlling the reaction stereoselectivity. In this example, the copper- and gold-catalyzed 1,3-phosphatyloxy and 1,3-halogen migration relay from α-halo-propargylic phosphates to stereodivergent 1,3-diene products.[26]

Propargylic esters[27,28] have attracted much attention, since they play an important part as highly valuable building blocks in modern organic chemistry.[29−32] With various catalysts, many new substances can be converted or functionalized from propargylic esters by cycloaddition,[33−36] cycloetherification,[37] amination, or rearrangement[38,39] reactions. Propagylic esters/phosphates with an additional adjacent functional group can undergo novel catalytic relay migrations, thereby producing functionalized 1,3-dienes. These double migrations are worthy in synthesis chemistry due to several merits:[40] (a) these kinds of double migratory processes can be catalyzed by simple and available catalysts; (b) high regio- and stereoselectivity can be achieved; (c) these cascade reactions show good compatibility of a variety of functional groups under different conditions; (d) the advantage for atom economy is that it allows one to build more complicated molecules rapidly including synthetically useful cyclic, acyclic, and polycyclic structures.[41,42]

The primitive research for double migration reaction began with a copper- or silver-catalyzed isomerization from propargylic acetates to allenyl acetates or 1,3-dienes.[43−45] Thereafter, zinc-,[46] palladium-,[47] and platinum-[48] catalyzed reactions were also developed. Recently, gold[49−51] complexes also emerged as distinctive catalysts for migration reactions, so this kind of catalysts is getting more and more attention.

The catalyzed double migration reaction can be started with a 1,3-ester (OXO, X = C(O) or $P(OEt)_2$) group migration from propargylic esters. Gevorgyan's group reported the gold-catalyzed cascade reaction of the propargylic esters and propargylic phosphates which undergoes the gold-catalyzed 1,3-acetate/phosphate migration and 1,2-alkyl migration sequence to produce 1,3-diene.[52−54] Interestingly, the gold-mediated 1,3-diene intermediates can subsequently lead to unsymmetrical naphthalenes by 6π-electrocyclization or Friedel−Crafts reactions.[52,54] Nevado and co-workers reported a gold-catalyzed cascade 1,3-acyloxy/1,3-alkyl migration of propargylic ester into cyclopentenylketone.[55] More mechanistic details on the reversibility of the 1,3-pivaloxy migration process were provided by Toste's group.[56] Then, they reported a method of gold-catalyzed enantioselective synthesis based on 1,3-pivaloxy/1,3-alkyl migration from propargylic pivalates to chromenyl derivatives with high enantioselectivity.[57] A copper-catalyzed 1,3-phosphatyloxy/1,2-H shift reaction from propargylic phosphates to five-membered heterocycles was reported by Gevorgyan's group.[58]

Received: November 14, 2014
Published: January 5, 2015

ACS Publications © 2015 American Chemical Society

DOI: 10.1021/jo502600j
J. Org. Chem. 2015, 80, 1661−1671

Besides 1,3-ester group migration, cascade migrations started by 1,2-ester group migration were also reported, including 1,2-OXO/1,2-H migration,[59,60] 1,2-OXO/1,4-allyl migration,[61−63] and 1,2-OXO/1,2-acyloxy migration.[29,64]

Most interestingly, Gevorgyan and co-workers recently reported a stereodivergent synthesis of highly functionalized (*Z*)-1,3-dienes (highlighted in blue, Scheme 1) and (*E*)-1,3-dienes (highlighted in red) from α-halo-propargylic phosphates via a 1,3-phosphatyloxy and 1,3-halogen migratory cascade reaction.[26] This reaction was suggested to start with an initial 1,3-OXO migration. Different from previous studies, after 1,3-OXO migration, a 1,3-halogen migration instead of 1,2-halogen migration underwent probably via a metal mediated carbon−halogen bond activation. A variety of cyclic-, acyclic-, and heterocyclic-containing substrates were converted into 1,3-dienes with efficiency. More importantly, there is a distinguished stereodivergence between copper and gold catalysis, of which the mechanistic origin was still unclear. It was found that the (*Z*)-dienes were obtained in the presence of a catalytic amount of $[CuOTf]_2$·PhH, while the use of a gold catalyst $(p\text{-}CF_3C_6H_4)_3PAuCl$ resulted in the formation of the corresponding (*E*)-dienes.

Scheme 1. Stereocontrolled 1,3-Phosphatyloxy and 1,3-Halogen Migration Relay toward Highly Functionalized 1,3-Dienes

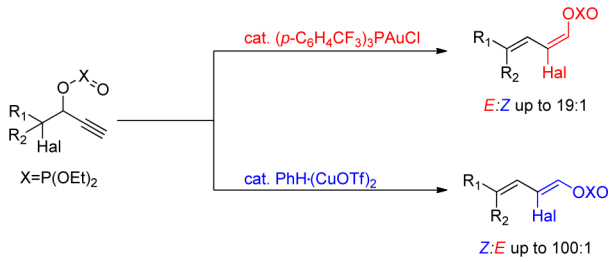

The reactions above have a common point that the transition metals play a role as Lewis acids to activate the alkynyl, and then mediate the activation of the carbon−halogen bond for subsequent migration. How does the character of the metal center influence these migration steps and control the stereochemistry of the catalysis? Herein, to address the distinctive mechanism of 1,3-OXO/1,3-halogen migration and the origin of stereodivergence between copper- and gold-catalyzed α-halo-propargylic phosphate to 1,3-dienes, we present a computational study with density functional theory (DFT) based on Gevorgyan's catalytic systems. This study demonstrates the importance of the metal center character, i.e., the hardness and softness, in tuning the stereoselectivity.

2. COMPUTATIONAL MODEL AND DETAILS

We applied a density functional theory (DFT) to investigate the reaction pathways of the Au- or Cu-catalyzed 1,3-phosphatyloxy and 1,3-halogen migration relay to 1,3-dienes, to study the geometries, electronic structures, and energetics along the reaction potential energy surfaces (PES). The effect of solvents (toluene for Au-catalyzed reaction and 1,2-dichloroethane for Cu-catalyzed reaction) on the reactions and stereoselectivities was considered with the integral equation formalism polarizable continuum medium[65] (IEF-PCM) model based on the optimized structures. All calculations were performed with the Gaussian 09 software package.[66]

When locating stationary and transition state structures in the gas phase, the DFT method with the B3LYP[67,68] (Becke's three-parameter hybrid, LYP correlation functional) functional was used. The relativistic LANL2DZ[69−71] was used for copper or gold. For the main-group atoms, the 6-311G(d) basis set was used for bromine, while the 6-31G(d) basis set was used for other elements (termed as BS1). Frequencies were calculated analytically at the same level of theory to confirm whether the structures were points on the local minima (no imaginary frequencies) or the first-order saddle points (transition states, only one imaginary frequency). Transition-state structures were

Scheme 2. Proposed Mechanism of Cascade Migratory Reaction

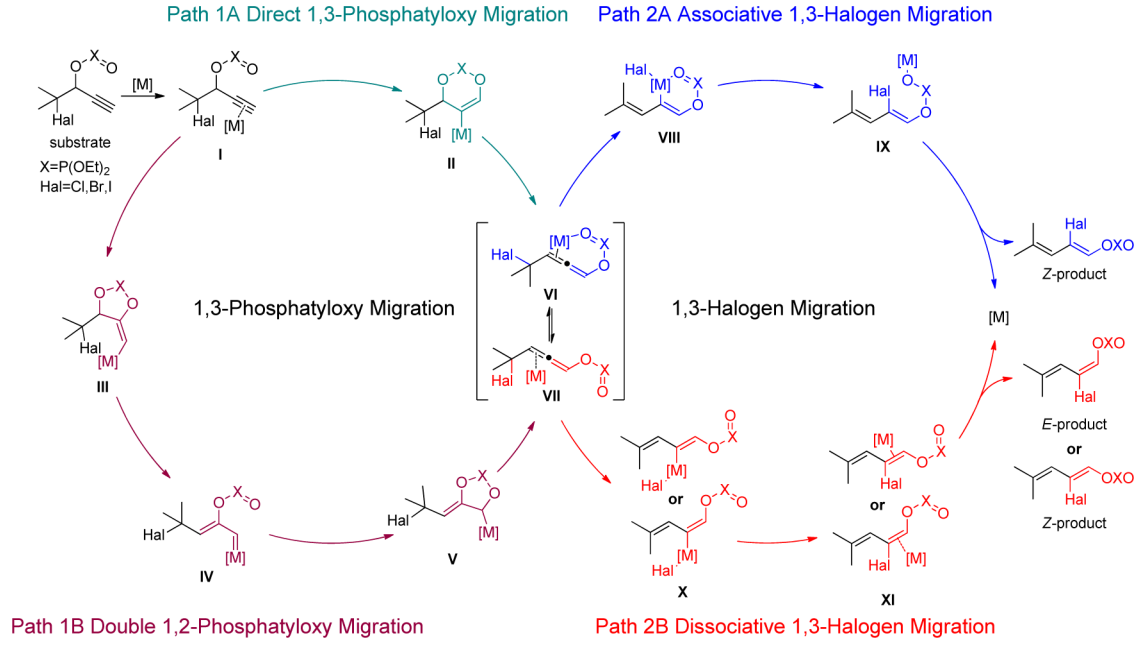

DOI: 10.1021/jo502600j
J. Org. Chem. 2015, 80, 1661−1671

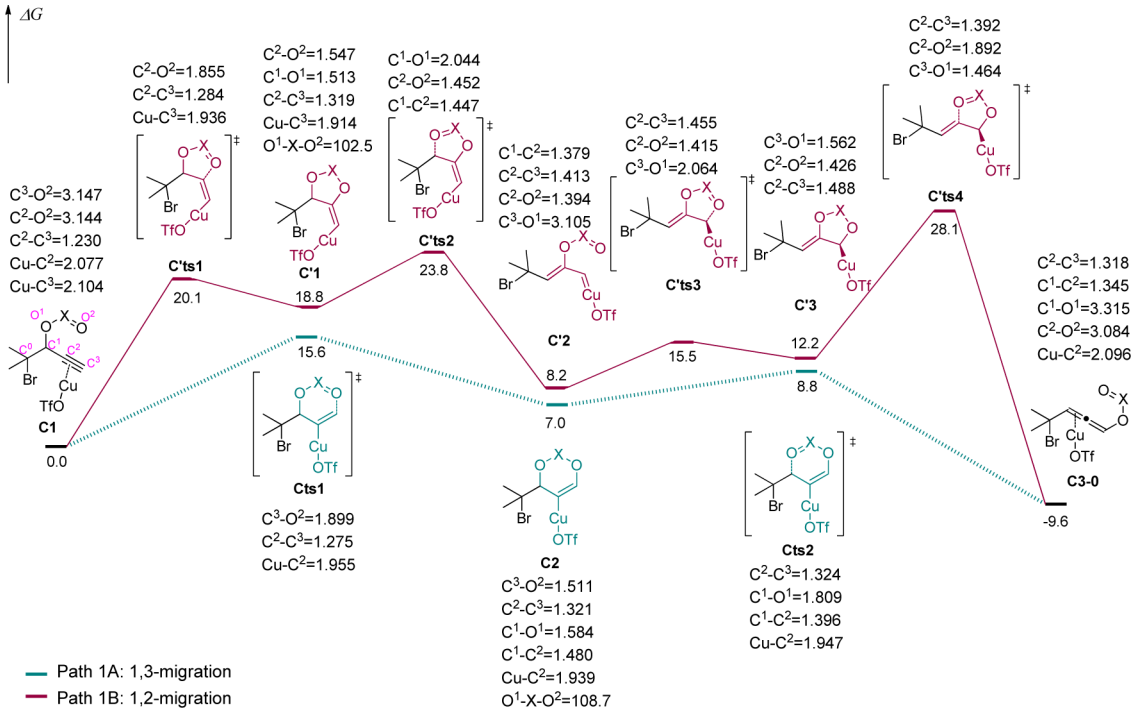

Figure 1. Free energy profiles for 1,3-phosphatyloxy migration of propargylic ester with copper catalyst in DCE. Relative bond lengths in Å, bond angles in deg, and Gibbs free energies in kcal/mol.

verified by intrinsic reaction coordinate (IRC) calculations to connect correct reactants and products.

In order to get better accuracy of the energetics, we further refined the single-point energies of the optimized geometries with a larger basis set, i.e., the LANL2DZ pseudopotential with outer p functions[72] and a set of f-polarization functions[73] for Cu or Au, and the 6-311+G(d,p) for the other atoms (called BS2). The parameters for toluene (ε = 2.379, for gold-catalyzed reaction) and 1,2-dichloroethane (DCE, ε = 10.36, for copper-catalyzed reaction) correspond to the experimental conditions. The radii from the UFF force field scaled by 1.1 with an explicit hydrogen radius were used in these calculations. The solvation free energies were obtained at the B3LYP/BS2/IEF-PCM//B3LYP/BS1 level of theory.

3. RESULTS AND DISCUSSION

The entire reaction involves two cascade migration steps (Scheme 2). The first one is metal-catalyzed 1,3-phosphatyloxy migration, which can be categorized as direct 1,3-phosphatyloxy migration (pathway 1A) and double 1,2-phosphatyloxy migration (pathway 1B). On pathway 1A, the metal center first coordinates to the alkynyl group of **I**, then undergoes a [3,3]-rearrangement of propargylic phosphate to cyclic intermediate **II**, followed by a C−O cleavage to form a metal-coordinated α-halo-allenyl-phosphate **VI**/**VII**. Likewise started from **I**, pathway 1B experiences a [2,3]-rearrangement of propargylic phosphate to five-membered cyclic intermediate **III**, leading to the formation of gold alkenyl carbenoid species **IV**, which undergoes another [2,3]-rearrangement to the α-halo-allenyl-phosphate **VI**/**VII** via another five-membered cyclic intermediate **V**. The second migration is metal-catalyzed 1,3-halogen migration initiated from **VI**/**VII**. According to the proposed mechanism, the migration may process via either an associative pathway (pathway 2A) or a dissociative pathway (pathway 2B). On pathway 2A, the metal center activates the C−Hal bond with the association of a coordinated phosphate group yielding the π-allyl intermediate **VIII**. A reductive elimination from **VIII** leads to the (*Z*)-1,3-diene associated by the phosphate group. On pathway 2B, the C−Hal bond activation is mediated by the metal center which is dissociative with respect to the phosphate group, to form π-allyl intermediate **X** from which a reductive elimination of the C−Hal bond leads to final products without the directing of the phosphate group.

To elucidate the mechanism and selectivity of the titled reactions, we chose the typical α-bromo-propargylic phosphate as a model reactant for study. Throughout our computational study, we chose the realistic P(p-$CF_3C_6H_4$)$_3$ and OTf^- ($CF_3SO_3^-$) ligands for the Au and the Cu catalysis, respectively. It should be noted that all discussed Au species are named with a capital **A** and Cu species with a capital **C**. As depicted in Figure 1, the carbon which links to the bromine atom is named C^0; then, from left to right, the rest of the three carbon atoms are named C^1, C^2, and C^3; likewise, the oxygen atoms in phosphate are named O^1 and O^2. To avoid confusion, all the given names of species are in bold.

3.1. 1,3-Phosphatyloxy Migration to α-Bromoallenyl Phosphate. The free energy profiles for the copper-catalyzed 1,3-phosphatyloxy migration to α-bromoallenyl phosphate are shown in Figure 1, via pathway 1A (**C1** → **Cts1** → **C2** → **Cts2** → **C3-0**) or pathway 1B (**C1** → **C′ts1** → **C′1** → **C′ts2** → **C′2**→ **C′ts3** → **C′3** → **C′ts4** → **C3-0**). From **C1** to **C2**, the activation free energy corresponding to the cyclization transition state **Cts1** is calculated to be 15.6 kcal/mol. Six-membered heterocycle **C2**, which is 7.0 kcal/mol higher in free energy than **C1**, undergoes a decyclization to the copper allenyl intermediate **C3-0** through transition state **Cts2** (8.8 kcal/mol). **C3-0** is 9.6 kcal/mol lower in free energy than **C1**. On pathway 1B, a five-membered intermediate **C′1**, transformed from **C1**, is highly unstable (18.8 kcal/mol higher in free energy than **C1**).

DOI: 10.1021/jo502600j
J. Org. Chem. 2015, 80, 1661−1671

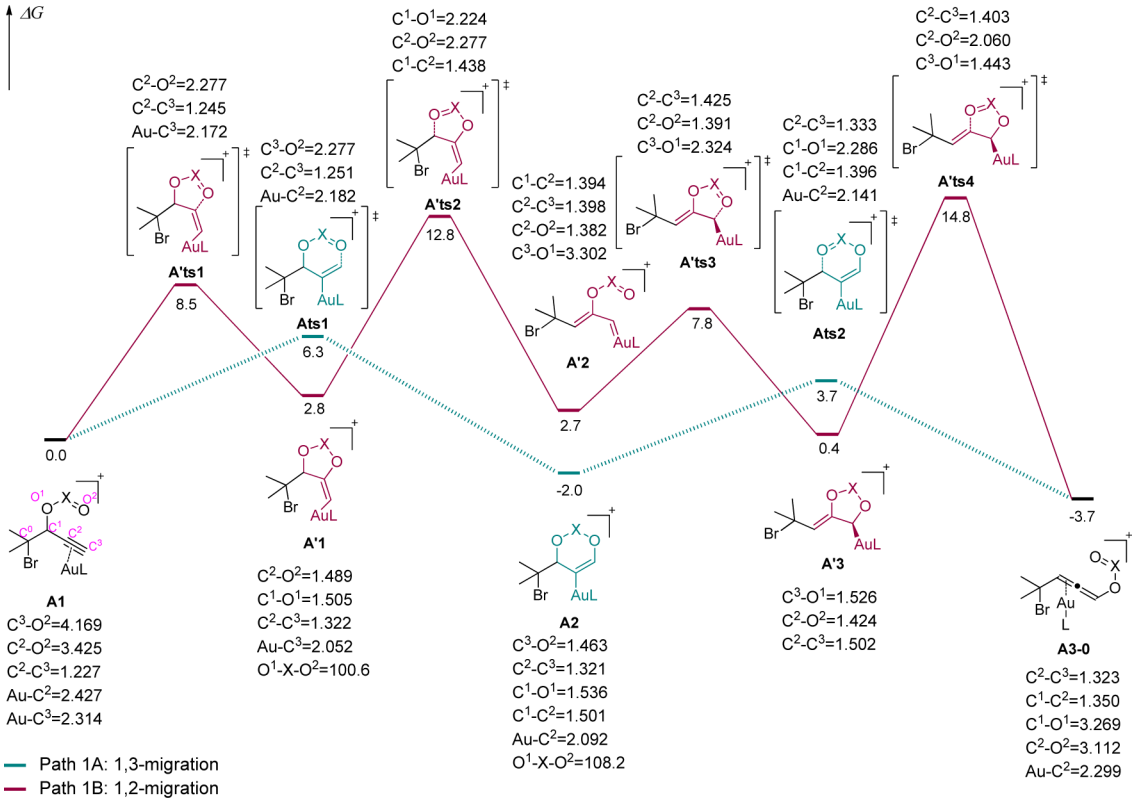

Figure 2. Free energy profiles for 1,3-phosphatyloxy migration of propargylic phosphate with gold complex (L = P(p-$C_6H_4CF_3$)$_3$) in toluene. Relative bond lengths in Å, bond angles in deg, and Gibbs free energies in kcal/mol.

Decyclization from intermediate **C′1** to the copper alkenyl carbenoid intermediate **C′2** has to overcome a free energy barrier of 23.8 kcal/mol through transition state **C′ts2**. **C′2** is 8.2 kcal/mol higher in free energy than **C1**. **C′2** proceeds another cyclization step to a five-membered heterocyclic species **C′3** (12.2 kcal/mol) via transition state **C′ts3** (15.5 kcal/mol). Subsequently, **C′3** proceeds to allenyl-coordinated species **C3-0** via transition state **C′ts4** with a free energy barrier of 28.1 kcal/mol.

With respect to the gold-catalyzed reaction, the Au-coordinated propargylic phosphate **A1** can also transform to the gold coordinated allene **A3-0** through the 1,3-phosphatyloxy migration pathway (pathway 1A: **A1** → **Ats1** → **A2** → **Ats2** → **A3-0**) or the double 1,2-phosphatyloxy migration pathway (pathway 1B: **A1** → **A′ts1** → **A′1** → **A′ts2** → **A′2** → **A′ts3** → **A′3**→ **A′ts4** → **A3-0**), as shown in Figure 2. Direct 1,3-phosphatyloxy migration (pathway 1A) starts from **A1** to the six-membered cyclic intermediate **A2** through transition state **Ats1** with a free energy barrier of 6.3 kcal/mol. Intermediate **A2**, which is more stable than the copper-mediated six-membered cyclic intermediate **C2**, since it is easier to stabilize the alkenyl group by the Au(I) center, is 2.0 kcal/mol lower in Gibbs free energy than **A1**. Subsequently, **A1** proceeds to allene-coordinated species **A3-0** via transition state **Ats2** with a free energy barrier of 5.7 kcal/mol. **A3-0** is 3.7 kcal/mol lower in free energy than **A1**. Another pathway, double 1,2-phosphatyloxy migration (pathway 1B), starts from **A1** to a five-membered cyclic intermediate **A′1**. This cyclization step goes through a higher transition state **A′ts1** with a free energy barrier of 8.5 kcal/mol. Intermediate **A′1** is 2.8 kcal/mol higher in Gibbs free energy than **A1**. Decyclization from **A′1** to the gold alkenyl carbenoid intermediate **A′2** goes through transition state **A′ts2** with a free energy barrier of 12.8 kcal/mol. **A′2** is 2.7 kcal/mol higher in free energy than **A1**. Through another cyclization step, **A′2** proceeds to a five-membered heterocyclic species **A′3** (0.4 kcal/mol) via transition state **A′ts3** (7.8 kcal/mol). Subsequent ring-opening of **A′3** leads to the formation of the gold allenyl species **A3-0** through transition state **A′ts4** with a free energy barrier of 14.8 kcal/mol.

Analysis from the above free energy profiles suggests that the direct 1,3-phosphatyloxy migration (pathway 1A) is more highly preferred than the double 1,2-phosphatyloxy migration pathway (pathway 1B) for both copper- and gold-catalyzed 1,3-phosphatyloxy migration reactions. For the copper-catalyzed 1,3-phosphatyloxy migration, the rate-determining transition state **C′ts4** (28.1 kcal/mol) of pathway 1B is much higher in free energy than that (**Cts1**, 15.6 kcal/mol) of pathway 1A. With respect to the gold-catalyzed 1,3-phosphatyloxy migration, the rate-determining transition state **A′ts4** (14.8 kcal/mol) of pathway 1B is also higher in free energy than that (**Ats1**, 6.3 kcal/mol) of pathway 1A. We can also see that nearly all the five-membered ring transition states of pathway 1B are higher in free energy than the six-membered ring transition states of pathway 1A for both the copper- and gold-catalyzed 1,3-phosphatyloxy migration reactions, as shown in Figures 1 and 2.

Insights can be seen from the transition state structures for this mechanistic difference between direct 1,3-phosphatyloxy migration (Figure 3) and double 1,2-phosphatyloxy migration (Figure S1, Supporting Information). **Cts1** and **Ats1** are six-membered transition states, in which the phosphate oxygen nucleophilically attacks the triple bond activated by Lewis acid (copper or gold). The bond distances between the nucleophilic oxygen atom and the terminal carbon atom in the propargylic

DOI: 10.1021/jo502600j
J. Org. Chem. 2015, 80, 1661−1671

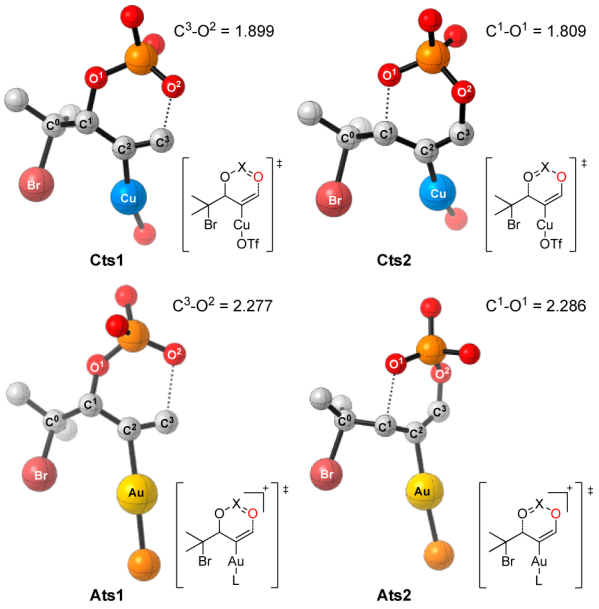

Figure 3. Optimized structures of transition states for 1,3-phosphatyloxy migration. Relative bond lengths in Å. (Triflyl, ethyl, and *p*-$CF_3C_6H_4$ groups and hydrogen atoms are omitted for clarity.)

phosphate (C^3-O^2) are 1.899 Å in **Cts1** for copper catalysis and 2.277 Å in **Ats1** for gold catalysis. It can be seen from the two figures above that **Ats1** is an early transition state, which is structurally closer to the starting species **A1** of the reaction coordinate than to the intermediate **A2**, whereas **Cts1** is a late transition state. According to the Hammond postulate,[74] early transition states are generally characteristic of rapid exothermic reactions and late transition states are generally characteristic of slow endothermic reactions; therefore, this postulate can explain that gold-catalyzed reactivity is higher than that of the copper-catalyzed reaction. In the following decyclization step, **C2** → **Cts2** → **C3-0** or **A2** → **Ats2** → **A3-0**, the cleavage of the C^1-O^1 bond completes the 1,3-phosphatyloxy migration to the allenyl intermediate via transition state **Cts2** or **Ats2**. The C^1-O^1 bond distances are 1.809 Å in **Cts2** and 2.286 Å in **Ats2**, respectively, which are comparable to the C^3-O^2 bond distances in **Cts1** and **Ats1**.

More specifically, bond angles O^1-X-O^2 are 108.7° in **C2** and 108.2° in **A2**, greater than that in **C′1** and **A′1** (102.5 and 100.6°, respectively); that is to say, pathway 1A is favored in 1,3-phosphatyloxy migration, because five-membered ring structures are more strained than six-membered ring structures so that five-membered ring structures are less stable.

3.2. Copper-Catalyzed 1,3-Bromine Migration. The subsequent 1,3-bromine migration starts from the allenyl intermediates yielded by 1,3-phosphatyloxy migration, **A3-0** and **C3-0**. There will be two different reaction pathways, i.e., the associative pathway 2A and the dissociative pathway 2B for copper mediated 1,3-bromine migration, as shown in Scheme 2. The *Z* product is exclusively obtained along the associative

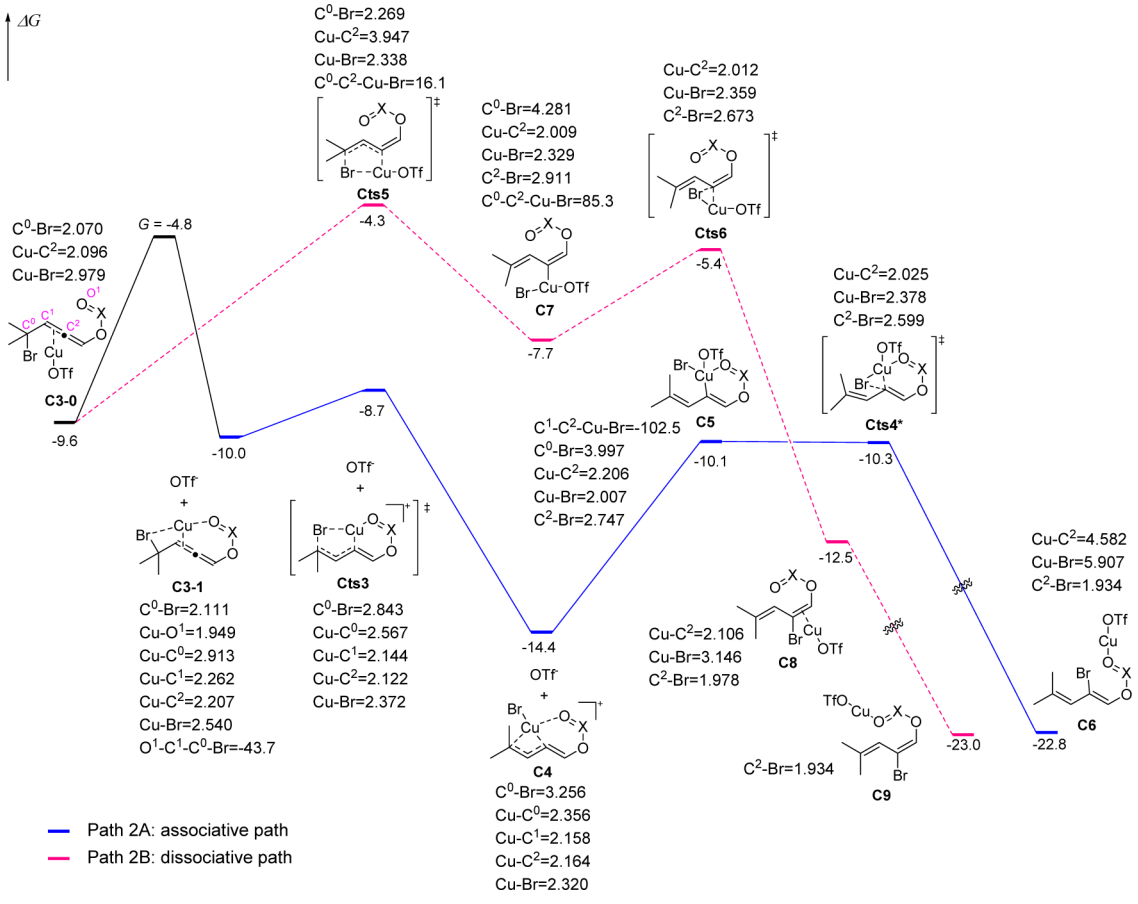

Figure 4. Free energy for copper-catalyzed 1,3-bromine migration in solvent (DCE). Relative bond lengths in Å, bond angles and dihedral angles in deg, and Gibbs free energies in kcal/mol. *The energy without zero point energy correction is higher than **C5** by 0.034 kcal/mol.

DOI: 10.1021/jo502600j
J. Org. Chem. 2015, 80, 1661−1671

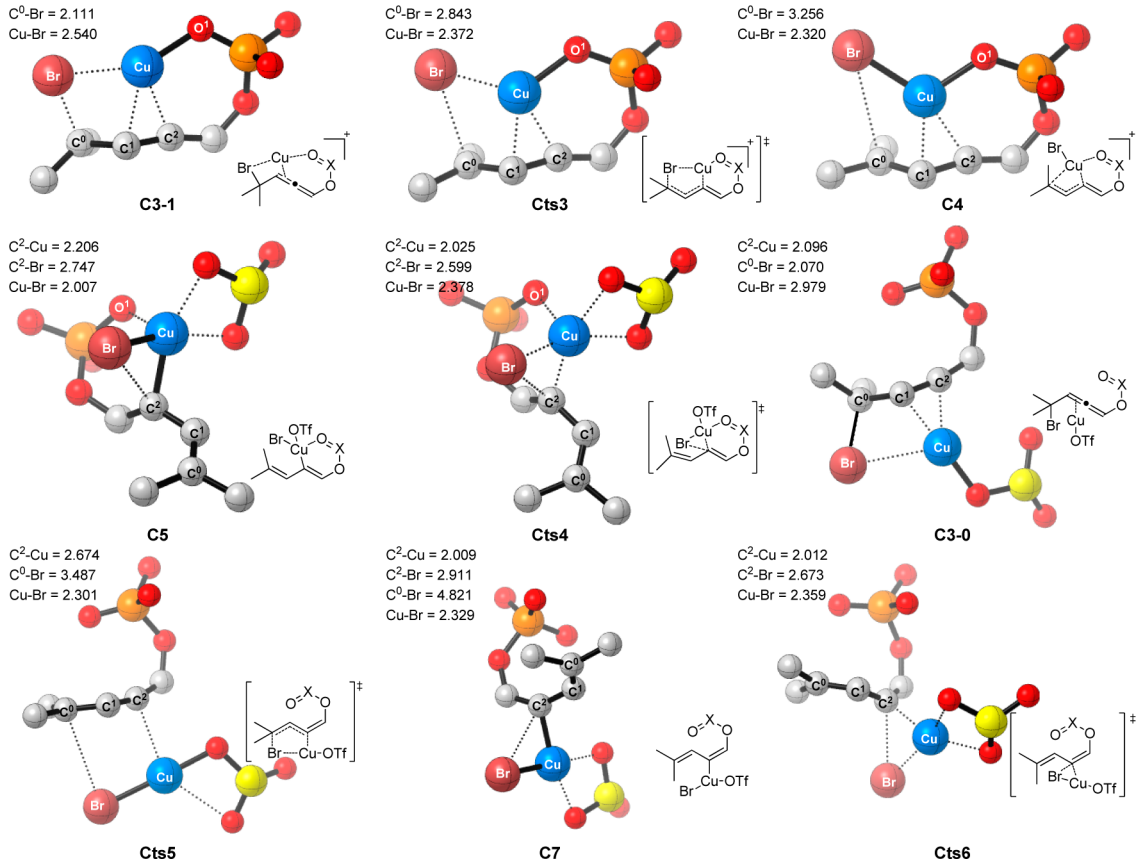

Figure 5. Schematic diagrams of the selected optimized geometries for mechanisms in copper-catalytic 1,3-bromine migration. Relative bond lengths in Å. (Ethyl and trifluoromethyl groups and hydrogen atoms are omitted for clarity.)

pathway, while both *E* and *Z* products are accessible on the dissociative pathway.

The copper-catalyzed 1,3-bromine migratory reaction starts from two isomers of **C3-0** and **C3-1** which are calculated to be −9.6 and −10.0 kcal/mol, respectively. **C3-0** and **C3-1** can be isomerized between each other. This isomerization between **C3-0** and **C3-1** involves Cu-double bond dissociation, Cu-OXO association, Cu-OTf^- dissociation, and Cu-double bond association. The rate-determining transition state for this isomerization is −4.8 kcal/mol (Figure S2, Supporting Information), suggesting that transformation between isomers **C3-0** and **C3-1** is easy in the solution. The oxidative addition of the C^0−Br bond to the copper center can undergo two kinds of transition states, **Cts3** and **Cts5**. The **Cts3** connects **C3-1** to the intermediate **C4** with a small free energy barrier of 1.3 kcal/mol, while the **Cts5** connects **C3-0** to **C7**, overcoming a higher activation free energy of 5.7 kcal/mol. The increased C^0−Br distances of 2.843 Å in **Cts3** and 3.487 Å in **Cts5** indicate the dissociation of Br from C^0, while the Cu−Br distances of 2.372 Å in **Cts3** and 2.301 Å in **Cts5** indicate the formation of Cu−Br bond to Cu(III) intermediate **C4** and **C7** (Figure 5).

It is noteworthy that the triflate anion does not participate in the associative pathway **C3-1** → **Cts3** → **C4** due to the association of the phosphate group to the copper center. The high reaction temperature (80 °C) required in experiment may entropically favor OTf^- dissociation. To further verify the dissociation of this triflate anion, we tried to find a similar associative pathway with coordinated OTf^- started from isomer **C3-2** via C^0−Br cleavage, finding out that the free energy of transition state **Cts3-2** with coordinated OTf^- is much higher than that of **Cts3** (see Figure S3 in the Supporting Information).

The subsequent reductive elimination of the C^2−Br bond starts with the isomerization of η^3-allylic intermediate **C4** to η^1-allylic intermediate **C5**, which requires the recoordination of the triflate anion onto the Cu center. **C5** can be converted to the product **C6** through a three-membered ring transition state **Cts4** with a small free energy barrier of 4.1 kcal/mol relative to **C4**. On the other hand, starting from the dissociative Cu(III) intermediate **C7**, a reductive elimination yields the (*Z*)-1,3-diene product via a three-membered ring transition state **Cts6**. The obtained **Cts6** is higher in free energy than **Cts4** by about 4.7 kcal/mol, although the distance of Cu−Br (2.378 Å) in **Cts4** is quite similar to that of **Cts6** (2.359 Å) during reductive elimination.

Throughout the entire free energy surface, we found that the highest transition state of 1,3-bromine migration for the associative pathway (**Cts3**) is lower in free energy than that of the dissociative pathway (**Cts5**) by 4.4 kcal/mol, as depicted in Figure 4. The associative reductive elimination transition state (**Cts4**) is also calculated to be lower than **Cts6** by 4.9 kcal/mol. These results indicate that the copper-catalyzed 1,3-bromine migration will selectively produce the *Z* product via the associative pathway with directing of the phosphate group, well consistent with the experimental observations.

Cu(I)/Cu(II) catalytic cycles, such as the single electron transfer (**SET**) mechanism and the halogen atom transfer (**HAT**) mechanism, are also considered as alternative pathways.[75,76] However, compared with the oxidative addition/

DOI: 10.1021/jo502600j
J. Org. Chem. 2015, 80, 1661−1671

reductive elimination mechanism, these two pathways are not favorable (see Figure S4, Supporting Information).

3.3. Gold-Catalyzed 1,3-Bromine Migration. With the understanding of stereoselectivity of the copper-catalyzed 1,3-bromine migration, we further illustrate the divergent stereoselective mechanism for the gold-catalyzed 1,3-bromine migration, by studying both the associative pathway and the dissociative pathway. The associative pathway to (*Z*)-1,3-diene is started from an intermediate **A3-0** (Figure 6). Structurally,

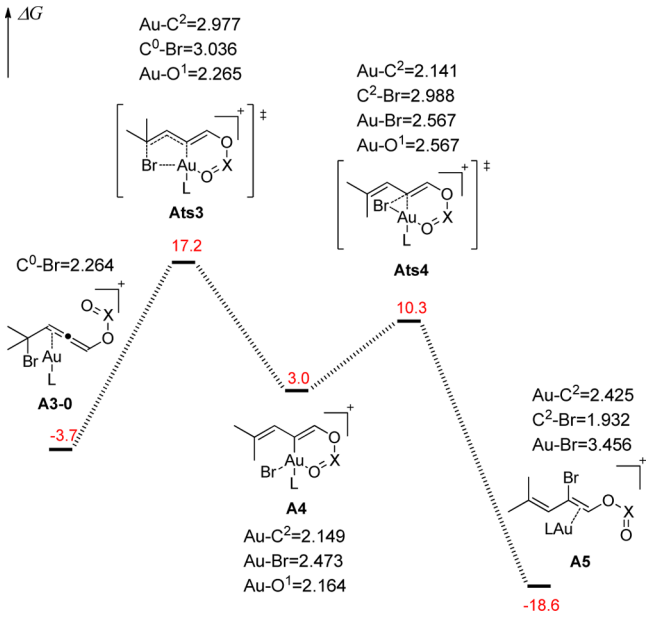

Figure 6. Free energy for gold-catalyzed associative 1,3-bromine migration (path 2A) in solvent (toluene). Relative bond lengths in Å, Gibbs free energies in kcal/mol. (L = P(*p*-$C_6H_4CF_3$)$_3$.)

the feature of this associative 1,3-migration is that the oxygen O^1 of phosphate coordinates to the Au center during oxidative addition of the C^0−Br bond, in contrast to the dissociative pathway where there is no Au−O^1 interaction (discussed below). The associative transition state, **Ats3**, is found to lead to an Au(III) intermediate **A4** with an activation free energy of 20.9 kcal/mol. Sequentially, another reductive elimination transition state structure **Ats4** (10.3 kcal/mol) is obtained for the formation of the C^2−Br bond to (*Z*)-1,3-diene **A5**.

On the other hand, the dissociative pathway of gold-catalyzed 1,3-bromine migration will lead to either *Z* type 1,3-diene or *E* type 1,3-diene, as shown in Scheme 2. The dissociative 1,3-bromine migration to (*Z*)-1,3-diene starts from intermediate **A3-1**, an isomer of **A3-0**. As shown in Figure 7, *Z*-type transition state **Ats5** connects **A3-1** to the Au(III) intermediate **A6-1**. The activation free energy of **Ats5** is 14.2 kcal/mol, lower than that of **Ats3** by 8.0 kcal/mol. First, the Au−Br distance 2.750 Å in **Ats5** reveals the formation of Au−Br bonding (Figure 8), while the increasing C^0−Br distance of 2.829 Å in **Ats5** shows the dissociation of Br from C^0. Second, in the process of **A3-1** → **Ats5** → **A6-1**, the gold center has changed into the oxidation state of Au(III), with the coordinate number of Au increasing to 4, and the value of bond angle C^2−Au−P^L is decreasing (158.4, 134.3, and 116.1°, respectively, where P^L is the phosphorus atom of the ligand). In another word, the η^2-allylic gold complex **A3-1** is transformed to the η^3-allylic species **A6-1** throughout the oxidative addition from Au(I) to Au(III). The isomerization of **A6-1** to intermediate **A6-2** (uphill by 3.3 kcal/mol) initiates the final step for this dissociative 1,3-migration, the C^2−Br reductive elimination. Intermediate **A6-2**, where the bromide is *cis* to the alkenyl group, goes through a three-membered transition state **Ats6** to the *Z* type product **A5**. **Ats6** processes a free energy barrier of 9.5 kcal/mol relative to **A1** and a reverse activation free energy of 28.1 kcal/mol relative to **A5**, respectively. After the reductive elimination, the Au(I) catalytic center is regenerated in **A5**, where the Au(I) center is linearly coordinated by phosphine and alkene.

To obtain the *E* type product (*E*)-1,3-diene, gold-catalyzed 1,3-bromine migration should undergo a stepwise dissociative pathway, which is similar to the pathway for the formation of (*Z*)-1,3-diene, via **A3-2** → **Ats7** → **A7-1** → **A7-2** → **Ats8** → **A8** (Figure 7). For the dissociative pathway to (*E*)-diene, structural parameters in oxidative addition transition state **Ats7** and reductive elimination transition state **Ats8** are very close to the ones of **Ats5** and **Ats6**, respectively. Relative to the starting point **A1**, the free energy of **Ats7** is 7.9 kcal/mol, which is lower by 1.3 kcal/mol than that of **Ats5** (9.2 kcal/mol). Thus, the oxidative addition of the C^0−Br bond with the phosphate group *trans* to the gold center (**Ats7**) is preferred over the one (**Ats5**) with the phosphate group *cis* to the gold center. **A7-2**, an isomer from **A7-1**, is calculated to be slightly less stable than **A7-1** by 3.4 kcal/mol in free energy. The three-membered reductive elimination transition state **Ats8**, which connects intermediate **A7-2** and product **A8**, has a calculated free energy of 7.5 kcal/mol, which is also lower than transition state **Ats6** (9.5 kcal/mol) with the gold center *cis* to the phosphate group. Hence, the dissociative pathway to the *E* product is more favorable than the dissociative pathway to the *Z* product. From this PES analysis, this conclusion is in good agreement with the experimental result that gold-catalyzed 1,3-bromine migration produces (*E*)-1,3-diene.

Therefore, for the pathway of obtaining 1,3-diene by the gold-catalyzed reaction, the dissociative pathways are more favored than that of the associative one, which is in contrast to the case of the copper-catalyzed reaction. The origin of this distinctive mechanistic difference will be further discussed in section 3.4 below.

3.4. The Origin of the Metal Effect on Stereoselectivity. As illustrated in sections 3.2 and 3.3, several important findings can be found by our detailed studies: (a) for copper-catalyzed 1,3-bromine migration, the associative pathway is more favored, which produces *Z* type 1,3-diene; (b) gold-catalyzed 1,3-bromine migration prefers the dissociative pathway to the associative pathway; (c) in the dissociative pathway of gold-catalyzed 1,3-bromine migration, the *E* product is preferred over the *Z* product. Consequently, two questions of interest require further illustration. First, why is the associative mechanism more favored for copper catalysis, whereas the dissociative pathway is more preferred for gold catalysis? Second, what is the origin of the *E* product selectivity for gold-catalyzed 1,3-bromine migration via the same dissociative pathway?

To understand the origin of the mechanistic difference, i.e., the associative or dissociative mechanism, that leads to the stereodivergence for copper and gold catalysts, we further analyze the coordination interaction between the Cu/Au center and the phosphate group. For the copper-catalyzed pathways, we found that the associative intermediate **C4** coordinated with the phosphate group is more stable than the dissociative one **C7** which is coordinated with a triflate anion by 6.7 kcal/mol.

DOI: 10.1021/jo502600j
J. Org. Chem. 2015, 80, 1661−1671

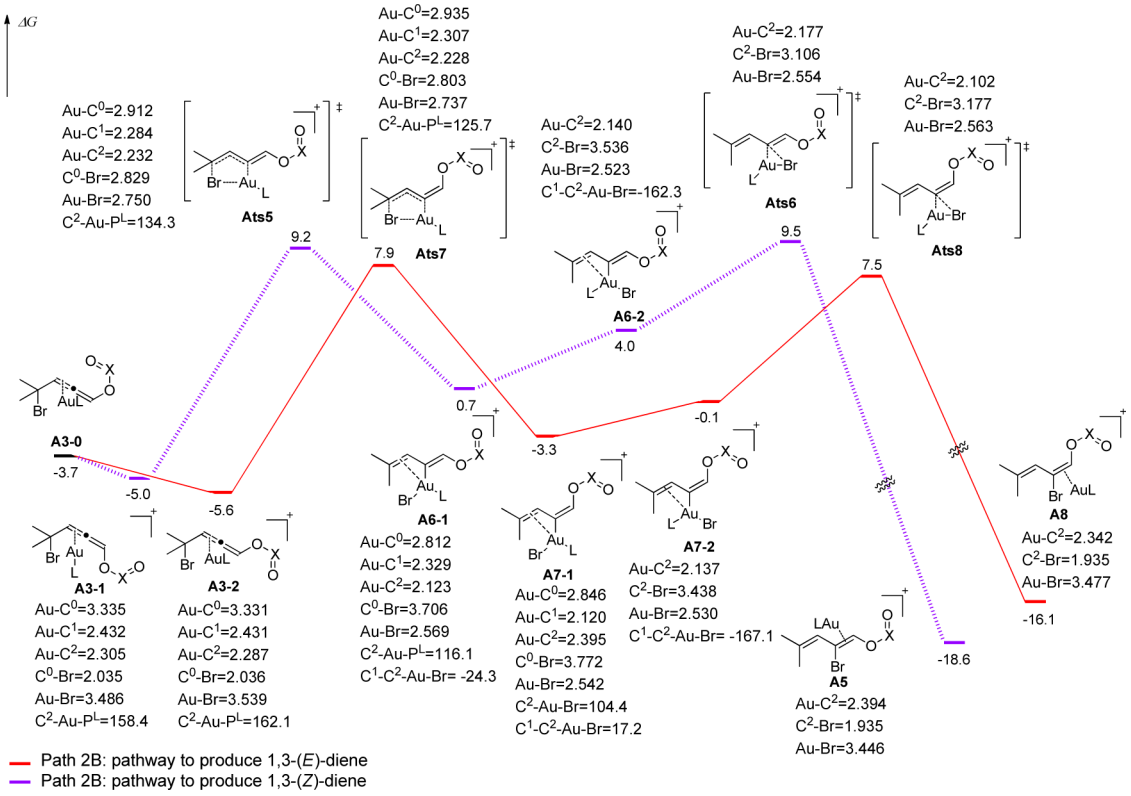

Figure 7. Free energy profiles for gold-catalyzed (L = P(p-$C_6H_4CF_3$)$_3$) dissociative 1,3-bromine migration in solvent (toluene). Relative bond lengths in Å, bond angles and dihedral angles in deg, and Gibbs free energies in kcal/mol.

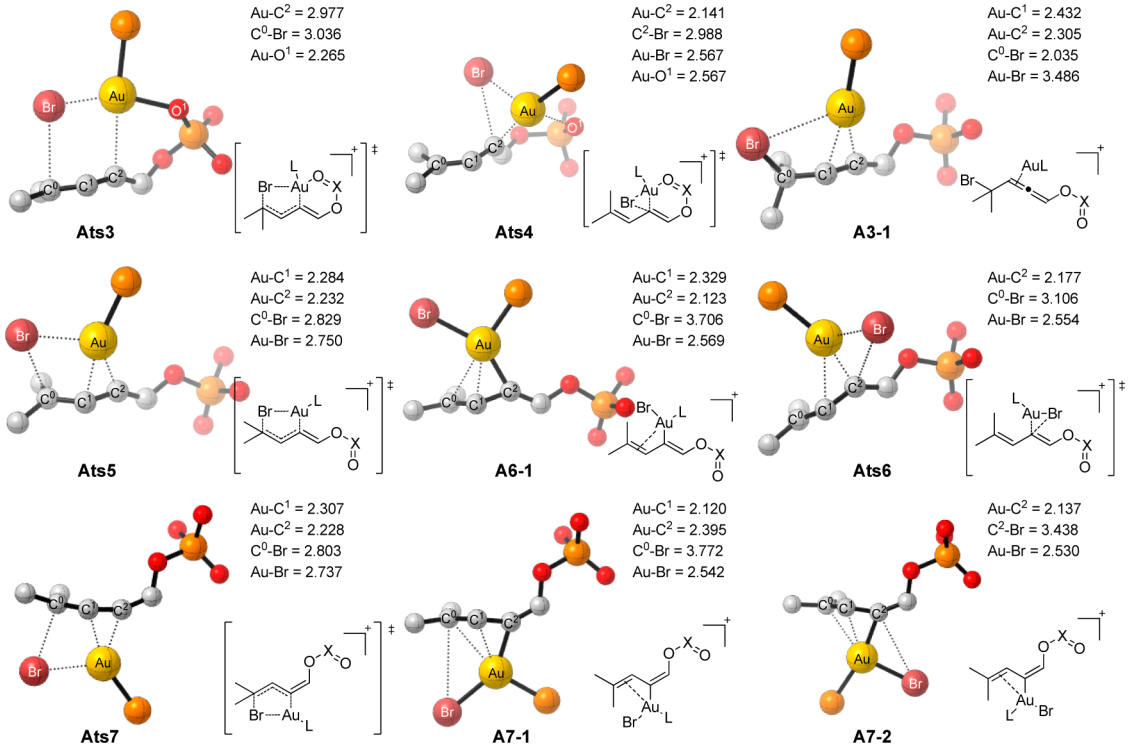

Figure 8. Schematic diagrams of the selected optimized geometries for mechanisms in gold-catalytic (L = P(p-$C_6H_4CF_3$)$_3$) 1,3-bromine migration. Relative bond lengths in Å. For charity, the phenyl substituents on the phosphine ligand, ethyl groups, and hydrogen atoms have been omitted in the figure.

This fact indicates that the Cu(III) prefers to coordinate with the phosphate group during the catalyzed 1,3-bromine migration. However, in the gold-catalyzed pathways, associative intermediate **A4** with the coordinated phosphate group is higher than dissociative intermediate **A6-1** by 2.3 kcal/mol in free energy, which suggests that the Au(III) center dislikes

DOI: 10.1021/jo502600j
J. Org. Chem. 2015, 80, 1661−1671

interacting with phosphate during 1,3-bromine migration reaction. These interesting discoveries can be rationalized by the HSAB theory. As pointed out by Pearson, soft acids react faster and form stronger bonds with soft bases, whereas hard acids react faster and form stronger bonds with hard bases.[1,6,7] A quantitative definition of the chemical hardness η can describe how hard or how soft the species are (see Table S1, Supporting Information).[77] Harder molecules have a larger η value, and softer species have a smaller one. Therefore, we used η to estimate the trend of coordinate energies relative to chemical hardness for corresponding ligands of interest.

As expected, the calculated chemical hardness of Cu(I) (η = 6.49 eV) is higher than that of Au(I) (η = 5.73 eV). Furthermore, after oxidative addition, the difference in hardness between these two metal centers in high oxidative states increases. Our calculation clearly indicates that Cu(III) (η = 9.04 eV) is much harder as compared with Au(III) (η = 5.97 eV). With respect to functional groups of reactants and ligands, we found that the phosphate group (η = 5.90 eV) is a harder base as compared to OTf^- (η = 5.00 eV) and phosphine ligand (η = 4.12 eV). In order to investigate the relationship between chemical hardness and ligand coordinate priority, we calculated several species of interest (Figure 9) at the B3LYP/BS2/IEF-

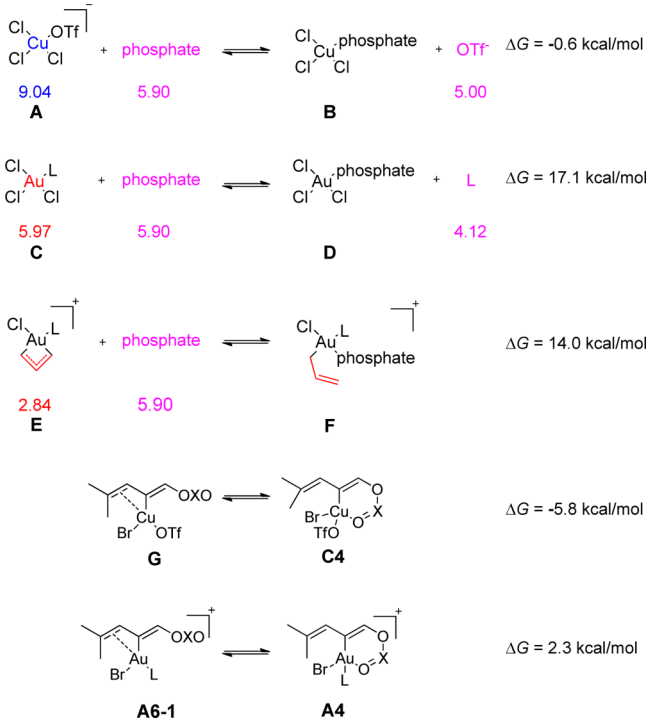

Figure 9. Calculated ligand exchanges for copper and gold complexes. Relative chemical hardness in eV. Values of chemical hardness are calculated at B3LYP/BS2 in the gas phase. (Phosphate = $P(O)(OEt)_3$, L = $P(p\text{-}C_6H_4CF_3)_3$, $\eta(Cu^{3+})$ = 9.04 eV, $\eta(Au^{3+})$ = 5.97 eV.)

PCM//B3LYP/BS1 level. As shown in Figure 9, the replacement of triflate anion with phosphate for the copper complex is exergonic by 0.6 kcal/mol. However, the replacement of phosphine ligand with phosphate for the gold complex is endergonic by 17.1 kcal/mol. We further compared the coordinate priority between the allyl group (η = 2.84 eV) and phosphate (η = 5.90 eV) for gold complexes. The results suggest that the substitution of one arm of the allyl group by phosphate is also endergonic by 14.0 kcal/mol. Obviously, the gold center prefers soft ligands to the hard phosphate ligand. On the basis of our calculation, copper intermediate **C4** with phosphate coordinated is more stable than the one (**G**) without phosphate by 5.8 kcal/mol. On the contrary, gold intermediate **A4** with phosphate coordinated is less stable than the one (**A6-1**) without phosphate by 2.1 kcal/mol. These results well support our hypothesis that the harder Cu(III) center prefers binding to harder bases (phosphate), whereas the softer Au(III) center disfavors binding to hard phosphate.

To further study the influence of ligand softness/hardness, we performed calculations on AuI catalyst, which has a weak coordinating iodide ligand. Our calculations (Figure S5, Supporting Information) indicate that, due to the softness of iodide, the AuI catalyst also prefers a dissociative pathway without coordination of pendant phosphate, and produces (*E*)-1,3-diene as the major product, which is in good agreement with experimental observation.[26]

3.5. The Origin of Stereoselectivity for Gold-Catalyzed Dissociative 1,3-Bromine Migration. We have revealed that the copper catalyst undergoes the associative pathway, leading exclusively to (*Z*)-diene. However, how does gold catalysis produce (*E*)-diene along the dissociative pathway without the directing of phosphate? To answer this question, it is necessary to analyze the features of the key transition states. As shown in Figure 10, the *cis* **Ats5** has more repulsion between the

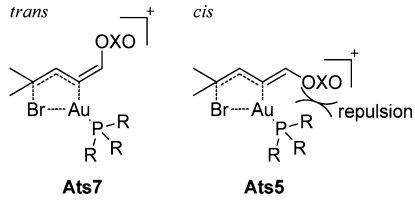

Figure 10. Steric effects on gold-catalyzed oxidative addition transition states for 1,3-bromine migration.

phosphate group and phosphine ligand than the *trans* **Ats7**, which leads to a free energy difference of 1.3 kcal/mol between **Ats7** and **Ats5**.

To further verify this hypothesis, we investigated model reactions with ligands bearing different bulky environments. Our results clearly suggest that the bulkier phosphine ligand leads to higher stereoselectivity. As shown in Figure 11, for the experimental studied ligand, $P(p\text{-}CF_3C_6H_4)_3$, the free energy of the *E* type transition state **Ets2** (Figure S6, Supporting Information) is lower than that of the *Z* type transition state **Zts2** by 1.2 kcal/mol (calculated at B3LYP/BS2). When a bulkier ligand like $P(t\text{-}Bu)_3$ is introduced, the *E*-selectivity increases with a calculated larger value of $\Delta\Delta G^{\ddagger}(\Delta G_{Zts}^{\ddagger} - \Delta G_{Ets}^{\ddagger})$ (2.3 kcal/mol). However, with a smaller phosphine (PMe_3) as the ligand, the *E* type oxidative addition transition state **Ets1** even becomes less stable than the *Z* type transition state **Zts1** by 1.1 kcal/mol. The trend of *E*:*Z* selectivity is well reflected by the structural features of the optimized transition states. The bond angle of Hn−Au−O^2, where Hn is the nearest hydrogen atom of phosphine to O^2, is found to be 48.3, 44.4, and 40.1° for **Zts1**, **Zts2**, and **Zts3**, respectively. In addition, we observed that the bond distances Hn−O^2 become shorter in *Z* type transition states when changing with more bulky phosphine (distances of Hn−O^2 are 2.908 Å in **Zts1**, 2.650 Å in **Zts2**, and 2.487 Å in **Zts3**, respectively). The smaller Hn−Au−O^2 angle and shorter Hn−O^2 distance indicate stronger repulsion between the phosphine ligand and the reactant, which

DOI: 10.1021/jo502600j
J. Org. Chem. 2015, 80, 1661−1671

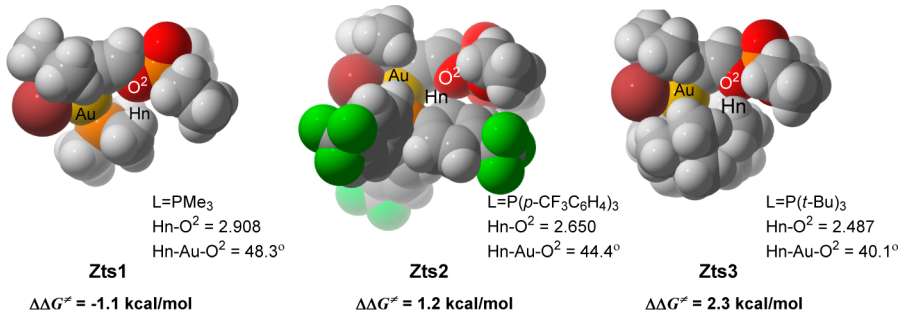

Figure 11. Optimized *cis* transition states (CPK model) for the oxidative addition step of gold-catalyzed 1,3-Br migration at the B3LYP/BS2 level with different bulky ligands (PMe_3, $P(p\text{-}CF_3C_6H_4)_3$, and $P(t\text{-}Bu)_3$), $\Delta\Delta G^{\ddagger} = \Delta G_{Zts}{}^{\ddagger} - \Delta G_{Ets}{}^{\ddagger}$. Relative bond lengths in Å, and bond angles in deg.

results in a less stable *Z* type transition state and higher *E*:*Z* selectivity. As a result, the steric effect plays an important role in the gold-catalyzed 1,3-bromine migration to achieve *E* types of stereoselectivity via the dissociative reaction pathway.

4. CONCLUSIONS

DFT studies have been performed to understand the stereoselective reaction mechanisms of Cu-catalyzed and Au-catalyzed 1,3-phosphatyloxy/1,3-bromine double migrations of α-bromine-substituted propargylic phosphates to 1,3-dienes with catalyst $[CuOTf]_2{\cdot}PhH$ and $(p\text{-}CF_3C_6H_4)_3PAuCl$, respectively.

The 1,3-phosphatyloxy migration catalyzed by copper or gold begins with the coordination of the metal to the triple bond of the alkyne, undergoing a Lewis acid induced 1,3-migration of the phosphatyloxy group to generate the six-membered cyclic intermediate, which upon elimination from the metal center produces allenyl phosphate. This 1,3-phosphatyloxy migration pathway has a calculated activation free energy of 15.6 and 8.5 kcal/mol for copper and gold catalysis, respectively. In contrast, a double 1,2-phosphatyloxy migration mechanism to allenyl phosphate is found to be less favorable for both copper and gold, of which the calculated activation free energies are 28.1 and 14.8 kcal/mol, respectively.

The 1,3-bromine migration step starts with the metal coordinated allenyl phosphate formed by 1,3-phosphatyloxy migration, and then undergoes an oxidative addition of the C−Br bond on to the metal center to an alkenyl phosphate intermediate, followed by a reductive elimination to selectively produce the final 1,3-dienes products. The copper-catalyzed 1,3-bromine migration proceeds an associative pathway, where the oxidative addition and reductive elimination are assisted with the coordinated phosphate group, leading predominately to the (*Z*)-1,3-diene. The calculated transition state energies for oxidative addition and reductive elimination in the dissociative pathway are both higher than those in the associative pathway by 4−5 kcal/mol. This is in good agreement with the experimental observation for copper catalyst.

In contrast, the Au-catalyzed 1,3-bromine migration prefers a dissociative pathway. The transition state of oxidative addition in the associative pathway is found to be 8.0 kcal/mol higher in free energy than that in the dissociative pathway. The origin of this stereodivergent mechanism can be well explained on the basis of the HSAB theory. The gold catalyst is relatively softer, while the copper catalyst is harder. During the 1,3-bromine migration, copper tends to interact with phosphatyloxy, whereas gold does not. The gold-catalyzed dissociative 1,3-bromine migration which produces (*E*)-1,3-diene instead of (*Z*)-1,3-diene is found to be controlled by the steric effect. The dissociative transition state of oxidative addition to (*E*)-1,3-diene is 1.3 kcal/mol lower than the transition state leading to (*Z*)-1,3-diene, which has strong repulsion between the phosphine ligand and phosphate group. These results well explain the opposite stereoselectivity of gold catalysis to copper catalysis observed experimentally.

The HSAB theory is widely applied in developing various catalytic reactivities and regioselectivities. Our study reveals the intriguing role of HSAB interaction in the stereodivergence of metal-catalyzed 1,3-phosphatyloxy/1,3-bromine double migrations, implying a promising strategy to tune the stereoselectivity of metal-catalyzed transformation based on the HSAB theory in the future.

■ ASSOCIATED CONTENT

Supporting Information

Complete ref 66, figures containing detailed information about other important structures, other PES profiles, chemical hardness data, and Cartesian coordinates. This material is available free of charge via the Internet at http://pubs.acs.org.

■ AUTHOR INFORMATION

Corresponding Author

*E-mail: kezhf3@mail.sysu.edu.cn

Notes

The authors declare no competing financial interest.

■ ACKNOWLEDGMENTS

This work was supported by NSFC funding (Grants 21203256, 21373277, and 21473261). Computing facilities were supported in part by the high performance grid computing platform of Sun Yat-sen University, the Guangdong Province Key Laboratory of Computational Science, and the Guangdong Province Computational Science Innovative Research Team.

■ REFERENCES

(1) Pearson, R. G. *J. Am. Chem. Soc.* **1963**, *85*, 3533.
(2) Pearson, R. G. *Inorg. Chem.* **1988**, *27*, 734.
(3) Pearson, R. G. *Proc. Natl. Acad. Sci. U. S. A.* **1986**, *83*, 8440.
(4) Pearson, R. G. *Science* **1966**, *151*, 172.
(5) Pearson, R. G.; Songstad, J. *J. Am. Chem. Soc.* **1967**, *89*, 1827.
(6) Pearson, R. G. *J. Chem. Educ.* **1968**, *45*, 581.
(7) Pearson, R. G. *J. Chem. Educ.* **1968**, *45*, 643.
(8) Silva, R. M.; Gwengo, C.; Lindeman, S. V.; Smith, M. D.; Gardinier, J. R. *Inorg. Chem.* **2006**, *45*, 10998.
(9) Chemaly, S. M.; Florczak, M.; Dirr, H.; Marques, H. M. *Inorg. Chem.* **2011**, *50*, 8719.
(10) Luo, T. T.; Hsu, L. Y.; Su, C. C.; Ueng, C. H.; Tsai, T. C.; Lu, K. L. *Inorg. Chem.* **2007**, *46*, 1532.

DOI: 10.1021/jo502600j
J. Org. Chem. 2015, 80, 1661−1671

(11) Yazaki, R.; Kumagai, N.; Shibasaki, M. *J. Am. Chem. Soc.* **2010**, *132*, 5522.
(12) Breugst, M.; Mayr, H. *J. Am. Chem. Soc.* **2010**, *132*, 15380.
(13) Mayr, H.; Breugst, M.; Ofial, A. R. *Angew. Chem., Int. Ed.* **2011**, *50*, 6470.
(14) Ho, T.-L. *Chem. Rev.* **1975**, *75*, 1.
(15) Geerlings, P.; De Proft, F.; Langenaeker, W. *Chem. Rev.* **2003**, *103*, 1793.
(16) Lopachin, R. M.; Gavin, T.; Decaprio, A.; Barber, D. S. *Chem. Res. Toxicol.* **2012**, *25*, 239.
(17) Holzweber, M.; Lungwitz, R.; Doerfler, D.; Spange, S.; Koel, M.; Hutter, H.; Linert, W. *Chem.—Eur. J.* **2013**, *19*, 288.
(18) Senanayake, G. *Hydrometallurgy* **2012**, *115*−*116*, 1.
(19) Zheng, J.; Tian, J.; Wu, D.; Gu, M.; Xu, W.; Wang, C.; Gao, F.; Engelhard, M. H.; Zhang, J. G.; Liu, J.; Xiao, J. *Nano Lett.* **2014**, *14*, 2345.
(20) (a) Chattaraj, P. K. *J. Phys. Chem. A* **2001**, *105*, 511. (b) Yamamoto, Y. *J. Org. Chem.* **2007**, *72*, 7817. (c) Jin, T.; Yamamoto, Y. *Org. Lett.* **2008**, *10*, 3137.
(21) Pinter, B.; Nagels, N.; Herrebout, W. A.; De Proft, F. *Chem.—Eur. J.* **2013**, *19*, 519.
(22) Salamone, M.; Mangiacapra, L.; DiLabio, G. A.; Bietti, M. *J. Am. Chem. Soc.* **2013**, *135*, 415.
(23) Méndez, F.; Romero, M. D. L.; Gazquez, J. L. *J. Chem. Sci.* **2005**, *117*, 525.
(24) (a) Ponti, A.; Molteni, G. *Chem.—Eur. J.* **2006**, *12*, 1156. (b) Xia, Y.; Dudnik, A. S.; Gevorgyan, V.; Li, Y. *J. Am. Chem. Soc.* **2008**, *130*, 6940.
(25) Damoun, S.; Van de Woude, G.; Choho, K.; Geerlings, P. *J. Phys. Chem. A* **1999**, *103*, 7861.
(26) Kazem Shiroodi, R.; Dudnik, A. S.; Gevorgyan, V. *J. Am. Chem. Soc.* **2012**, *134*, 6928.
(27) Marco-Contelles, J.; Soriano, E. *Chem.—Eur. J.* **2007**, *13*, 1350.
(28) Marion, N.; Nolan, S. P. *Angew. Chem., Int. Ed.* **2007**, *46*, 2750.
(29) Huang, X.; de Haro, T.; Nevado, C. *Chem.—Eur. J.* **2009**, *15*, 5904.
(30) Liu, H.; Li, X.; Chen, Z.; Hu, W. X. *J. Org. Chem.* **2012**, *77*, 5184.
(31) Yang, J.-M.; Zhang, Z.; Wei, Y.; Shi, M. *Tetrahedron Lett.* **2012**, *53*, 6173.
(32) Yoshida, M.; Nakagawa, T.; Kinoshita, K.; Shishido, K. *J. Org. Chem.* **2013**, *78*, 1687.
(33) Cai, S.; Liu, Z.; Zhang, W.; Zhao, X.; Wang, D. Z. *Angew. Chem., Int. Ed.* **2011**, *50*, 11133.
(34) Gung, B. W.; Bailey, L. N.; Wonser, J. *Tetrahedron Lett.* **2010**, *51*, 2251.
(35) Conyers, R. C.; Gung, B. W. *Chem.—Eur. J.* **2013**, *19*, 654.
(36) Iqbal, N.; Fiksdahl, A. *J. Org. Chem.* **2013**, *78*, 7885.
(37) De Brabander, J. K.; Liu, B.; Qian, M. *Org. Lett.* **2008**, *10*, 2533.
(38) Barluenga, J.; Riesgo, L.; Vicente, R.; Lopez, L. A.; Tomas, M. *J. Am. Chem. Soc.* **2007**, *129*, 7772.
(39) Wang, S.; Zhang, L. *J. Am. Chem. Soc.* **2006**, *128*, 8414.
(40) Kazem Shiroodi, R.; Gevorgyan, V. *Chem. Soc. Rev.* **2013**, *42*, 4991.
(41) Trost, B. M. *Angew. Chem., Int. Ed.* **1995**, *34*, 259.
(42) Trost, B. M. *Science* **1991**, *254*, 1471.
(43) Cookson, R. C.; Cramp, M. C.; Parsons, P. J. *J. Chem. Soc., Chem. Commun.* **1980**, 197.
(44) Saucy, G.; Marbet, R.; Lindlar, H.; Isler, O. *Helv. Chim. Acta* **1959**, *42*, 1945.
(45) Schlossarczyk, H.; Sieber, W.; Hesse, M.; Hansen, H.-J.; Schmid, H. *Helv. Chim. Acta* **1973**, *56*, 875.
(46) Strickler, H.; Davis, J. B.; Ohloff, G. *Helv. Chim. Acta* **1976**, *59*, 1328.
(47) Rautenstrauch, V. *J. Org. Chem.* **1984**, *49*, 950.
(48) Mainetti, E.; Mouriès, V.; Fensterbank, L.; Malacria, M.; Marco-Contelles, J. *Angew. Chem., Int. Ed.* **2002**, *41*, 2132.
(49) Mamane, V.; Gress, T.; Krause, H.; Furstner, A. *J. Am. Chem. Soc.* **2004**, *126*, 8654.
(50) Shi, X.; Gorin, D. J.; Toste, F. D. *J. Am. Chem. Soc.* **2005**, *127*, 5802.
(51) Zhang, L. *J. Am. Chem. Soc.* **2005**, *127*, 16804.
(52) Dudnik, A. S.; Schwier, T.; Gevorgyan, V. *Org. Lett.* **2008**, *10*, 1465.
(53) Dudnik, A. S.; Schwier, T.; Gevorgyan, V. *J. Organomet. Chem.* **2009**, *694*, 482.
(54) Dudnik, A. S.; Schwier, T.; Gevorgyan, V. *Tetrahedron* **2009**, *65*, 1859.
(55) Zou, Y.; Garayalde, D.; Wang, Q.; Nevado, C.; Goeke, A. *Angew. Chem., Int. Ed.* **2008**, *47*, 10110.
(56) Mauleon, P.; Krinsky, J. L.; Toste, F. D. *J. Am. Chem. Soc.* **2009**, *131*, 4513.
(57) Wang, Y. M.; Kuzniewski, C. N.; Rauniyar, V.; Hoong, C.; Toste, F. D. *J. Am. Chem. Soc.* **2011**, *133*, 12972.
(58) Schwier, T.; Sromek, A. W.; Yap, D. M.; Chernyak, D.; Gevorgyan, V. *J. Am. Chem. Soc.* **2007**, *129*, 9868.
(59) Li, G.; Zhang, G.; Zhang, L. *J. Am. Chem. Soc.* **2008**, *130*, 3740.
(60) Cho, E. J.; Lee, D. *Adv. Synth. Catal.* **2008**, *350*, 2719.
(61) Davies, P.; Albrecht, S. *Synlett* **2011**, *2012*, 70.
(62) Uemura, M.; Watson, I. D.; Katsukawa, M.; Toste, F. D. *J. Am. Chem. Soc.* **2009**, *131*, 3464.
(63) Davies, P. W.; Albrecht, S. J. *Chem. Commun.* **2008**, 238.
(64) de Haro, T.; Gomez-Bengoa, E.; Cribiu, R.; Huang, X.; Nevado, C. *Chem.—Eur. J.* **2012**, *18*, 6811.
(65) Tomasi, J.; Mennucci, B.; Cammi, R. *Chem. Rev.* **2005**, *105*, 2999.
(66) Frisch, M. J.; et al. *Gaussian 09*, revision B.01; Gaussian, Inc.: Wallingford, CT, 2010.
(67) Lee, C.; Yang, W.; Parr, R. G. *Phys. Rev. B* **1988**, *37*, 785.
(68) Becke, A. D. *J. Chem. Phys.* **1993**, *98*, 5648.
(69) Hay, P. J.; Wadt, W. R. *J. Chem. Phys.* **1985**, *82*, 299.
(70) Hay, P. J.; Wadt, W. R. *J. Chem. Phys.* **1985**, *82*, 270.
(71) Wadt, W. R.; Hay, P. J. *J. Chem. Phys.* **1985**, *82*, 284.
(72) Couty, M.; Hall, M. B. *J. Comput. Chem.* **1996**, *17*, 1359.
(73) Ehlers, A. W.; Böhme, M.; Dapprich, S.; Gobbi, A.; Höllwarth, A.; Jonas, V.; Köhler, K. F.; Stegmann, R.; Veldkamp, A.; Frenking, G. *Chem. Phys. Lett.* **1993**, *208*, 111.
(74) Hammond, G. S. *J. Am. Chem. Soc.* **1955**, *77*, 334.
(75) Jones, G. O.; Liu, P.; Houk, K. N.; Buchwald, S. L. *J. Am. Chem. Soc.* **2010**, *132*, 6205.
(76) Zhang, S.; Zhu, Z.; Ding, Y. *Dalton Trans.* **2012**, *41*, 13832.
(77) Delchev, Y. I.; Kuleff, A. I.; Maruani, J.; Mineva, T.; Zahariev, F. Strutinsky's Shell-Correction Method in the Extended Kohn-Sham Scheme: Application to the Ionization Potential, Electron Affinity, Electronegativity and Chemical Hardness. In *Recent Advances in the Theory of Chemical and Physical Systems*; Julien, J.-P., Maruani, J., Mayou, D., Wilson, S., Delgado-Barrio, G., Eds.; Springer: Dordrecht, The Netherlands, 2006; p 159.

DOI: 10.1021/jo502600j
J. Org. Chem. 2015, 80, 1661−1671